JMEPEG (2019) 28:1132–1140
https://doi.org/10.1007/s11665-018-3843-3

1059-9495/$19.00

Enhanced Surface Properties and Microstructure Evolution of Cr12MoV Using Ultrasonic Surface Rolling Process Combined with Deep Cryogenic Treatment

Shuai Ren, Yunfei Zhang, Yingli Zhao, Zhiguo An, Feng Xue, Jitan Yao, Zhiyan Sun, and Jinbao Chang

(Submitted April 15, 2018; in revised form September 8, 2018; published online January 2, 2019)

In this study, the enhanced surface properties and microstructure evolution of quenched and tempered cold work die steel Cr12MoV, which were induced by ultrasonic surface rolling process combined with deep cryogenic treatment (UDCT), were systematically investigated. The results indicated that UDCT had an advantage over conventional ultrasonic surface rolling process (USRP) in improving surface mechanical properties, including smaller surface roughness and smoother machined surface with less cracks and defects; higher surface microindentation hardness with the value of ~ 890 HV (increased by ~ 6.2% compared with USRP); and lower friction coefficient. Such enhancements in surface properties are mainly attributed to the martensitic transformation of retained austenite, the dispersion strengthening of small secondary carbides and the homogenized carbides distribution during UDCT.

Keywords nano-processing, rolling, steel, ultra-high strength

1. Introduction

Ultrasonic surface rolling process (USRP) has attracted wide attention over decades since it can significantly enhance the surface properties of materials. It shows great potential in improving the tensile strength, microindentation hardness, wear resistance and fatigue strength of materials (Ref 1, 2). During USRP, the surface of the sample is struck by a tungsten carbide ball attached to an ultrasonic device vibrating at high frequency. Thus, excellent microstructure, surface quality, hardness and residual compressive stress are received during the process (Ref 3, 4). Recently, USRP has been widely used to improve the wear resistance and fatigue life of materials (Ref 5, 6). Li et al. (Ref 3) investigated the wear properties of Ti-6Al-4V alloy under USRP with different frequencies and proposed that the wear properties were remarkably enhanced due to the ultra-refined grains. Wang et al. (Ref 7) investigated the nano-crystallization of 40Cr during USRP and indicated that USRP could improve the wear resistance of workpiece. Huang et al. (Ref 8) indicated that the fatigue strength of AISI 316L stainless steel was significantly enhanced in both the low- and high-cycling fatigue regimes after USRP. Pileups with various shapes and sizes were easily formed when severe impact was applied on the surface (Ref 9). Remarkable work hardening in surface strength layer induced by USRP restricts its further plastic deformation inside the material (Ref 10). Electro-pulsing-assisted USRP was applied for improving the ductility of materials (Ref 11-13). This method has shown a good application in promoting plastic deformation ability, improving recrystallization, cracks healing and so on (Ref 14-16). For Cr12MoV cold work die steel, the good surface mechanical properties are exactly needed. Generally, high performance always means high requirements for ultrasonic rolling equipment, especially for the quenched and tempered Cr12MoV with very high hardness. Electro-pulsing-assisted USRP may be suitable for machining Cr12MoV. However, during electro-pulsing-assisted USRP, the electro-pulsing, as an instantaneous high-energy input source, could lead to a temperature rise due to the effect of Joule heating. Excessive temperature would have unfavorable effects on the performance of Cr12MoV. Therefore, another method should be found which can be applied together with USRP to enhance the surface properties of Cr12MoV.

Deep cryogenic treatment (DCT) is another effective method to promote the mechanical properties of Cr12MoV. In this method, the material is held at a cryogenic temperature for a given soaking time and then heated to room temperature to improve the mechanical properties (Ref 17). Compared with normal heat treatment, the hardness, toughness, wear resistance and fatigue behavior could be further enhanced by DCT. The enhancements achieved by DCT are beyond the enhancements obtained by normal heat treatment (Ref 18, 19). Interesting positive effects were noted in maraging steel (Ref 20), tool steels (Ref 21-23), cast iron (Ref 24), tungsten carbide (Ref 25) and carburized steel (Ref 26). Amini et al. (Ref 27) pointed out that with respect to normal heat treatment, the wear resistance of 80CrMo12 5 cold work steel was improved by 37-52% due to DCT. Thornton et al. (Ref 28) reported that in comparison with normal heat treatment, DCT improved wear resistance of gray cast iron by 9.1-81.4% under the wear conditions. By means of both laboratory tests and field tests on real tools, Molinari et al. (Ref 29) indicated that DCT improved wear resistance of AISI M2 and AISI H13 steel even more than traditional heat treatment. Dong et al. (Ref 30) demonstrated that DCT doubled the service life of AISI M2 milling cutters. Above all the studies mentioned, the pretreatment of DCT is a

Shuai Ren, Yunfei Zhang, Yingli Zhao, Zhiguo An, Feng Xue, Jitan Yao, Zhiyan Sun, and **Jinbao Chang**, HBIS Group Technology Research Institute, Shijiazhuang 050000, People's Republic of China. Contact e-mail: hegangrenshuai@126.com.

traditional heat treatment. USRP has rarely been reported as a pre-DCT process.

In the present work, USRP combined with DCT (UDCT) was applied to the quenched and tempered cold work die steel Cr12MoV, to obtain excellent surface mechanical properties. At the same time, the mechanism for the influence of UDCT on surface mechanical properties and microstructure evolution was investigated.

2. Experimental

2.1 Materials and Processing Technique

The quenched and tempered Cr12MoV bars were investigated as original studied materials. The quenching and tempering temperatures were 1030 and 200 °C, respectively. The chemical composition of the as-used Cr12MoV is shown in Table 1. Turning process was performed before USRP and UDCT to obtain uniform sample dimensions ($\varphi 15 \times 150$ mm) and surface morphology characteristics as much as possible. The cutting parameters were as follows: cutting speed (26.0 m/min), feeding rate (60 mm/min).

USRP was carried out on a self-designed platform based on a CNC lathe. Figure 1 shows the configuration of USRP device. It consists of two parts: USRP operator and ultrasonic wave generator; the former part includes piezoelectric ceramic energy transducer, amplitude changing rod and scrollable rolling tip with hardness of more than 90 HRA, surface roughness of Ra 0.1 and radius of curvature of 6 mm. During USRP, ultrasonic vibration and static force were applied on workpiece surface in normal direction. The combination of ultrasonic vibration and static force leads to serve plastic deformation, which would inevitably make the original grains within subsurface region crushed heavily. A uniform, fine and large-thickness strengthened layer can be obtained by repeating the USRP. The parameters of USRP are presented in Table 2. Samples were repeatedly machined for 3 times to obtain uniform strengthened layers. After USRP, DCT was carried out by gradually cooling the samples to − 196 °C and holding the samples at this temperature for 3 h, followed by uniform heating to room temperature.

2.2 Measuring and Characterizing

The surface roughness of turning, USRP and UDCT samples was evaluated by a Mitutoyo SJ-210 portable surface roughness tester. The microindentation hardness of strengthened layers was measured by using a Tukon2500Minuteman digital sclerometer under an applied load of 200 g for 15 s. At least 15 measurements for each sample were taken to obtain an average microindentation hardness value. The microstructure of sample surfaces along depth after USRP and UDCT was analyzed by utilizing Zeiss Ultra 55 scanning electron microscope (SEM) and Zeiss Lsm700 laser scanning confocal microscope. The contents of the retained austenite (RA) and martensite of the samples before and after DCT were measured using XRD with the PANalytical Empyrean x-ray diffraction instrument that uses a Cu Kα x-ray source. Friction and wear tests were carried out on self-designed friction and wear testing machine at room temperature. The linear cutting machine was used to prepare the friction and wear testing samples, and the friction pair was quenched Cr12MoV. The weight loss of turning, USRP and UDCT samples after friction was measured by FA2004 top loading electronic balance.

3. Results

3.1 Surface Roughness

The axial surface roughness and morphology of turning, USRP and UDCT samples are shown in Fig. 2. The mean value of surface roughness of the turning samples is about Ra 1.089 μm, as shown in Fig. 2(a). A remarkable reduction in the surface roughness is obtained after USRP is applied with the surface roughness value of Ra 0.284 μm, as shown in Fig. 2(b). Meanwhile, it can be seen that some fluctuations, which would restrict its further improvement of surface roughness, still exist at certain positions on the surface roughness curve of USRP sample. The surface roughness further decreases to Ra 0.265 μm when UDCT is applied, as shown in Fig. 2(c). Furthermore, a more uniform surface roughness curve with fewer fluctuations is obtained compared with Fig. 2b. A careful comparison among Fig. 2(a′), (b′) and (c′) reveals some obvious morphology differences at microlevel. During the turning process, there exists a serve plastic shear deformation due to the serious work hardening in the cutting area on the surface of Cr12MoV, resulting in apparent turning marks (Fig. 2a′). It is certain that cracks would propagate along these turning marks during the use of the Cr12MoV workpiece, thus

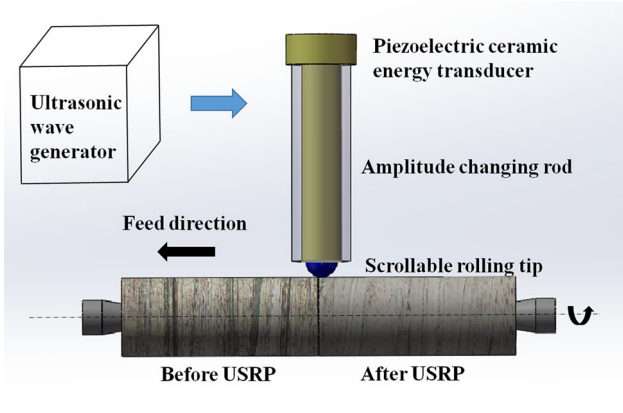

Fig. 1 Schematic diagram of the USRP working

Table 1 Chemical composition of Cr12MoV

Elements	Fe	C	Si	Mn	P	S	Cr	Mo	V
wt.%	Bal.	1.51	0.275	0.369	0.008	0.005	11.97	0.53	0.29

Table 2 Processing parameters of USRP

Rolling line speed, m/min	Feeding rate, mm/min	Frequency, kHz	Static force, N	Processing length, mm	Vibration amplitude, μm
7.4	0.1	30	1246	60	6

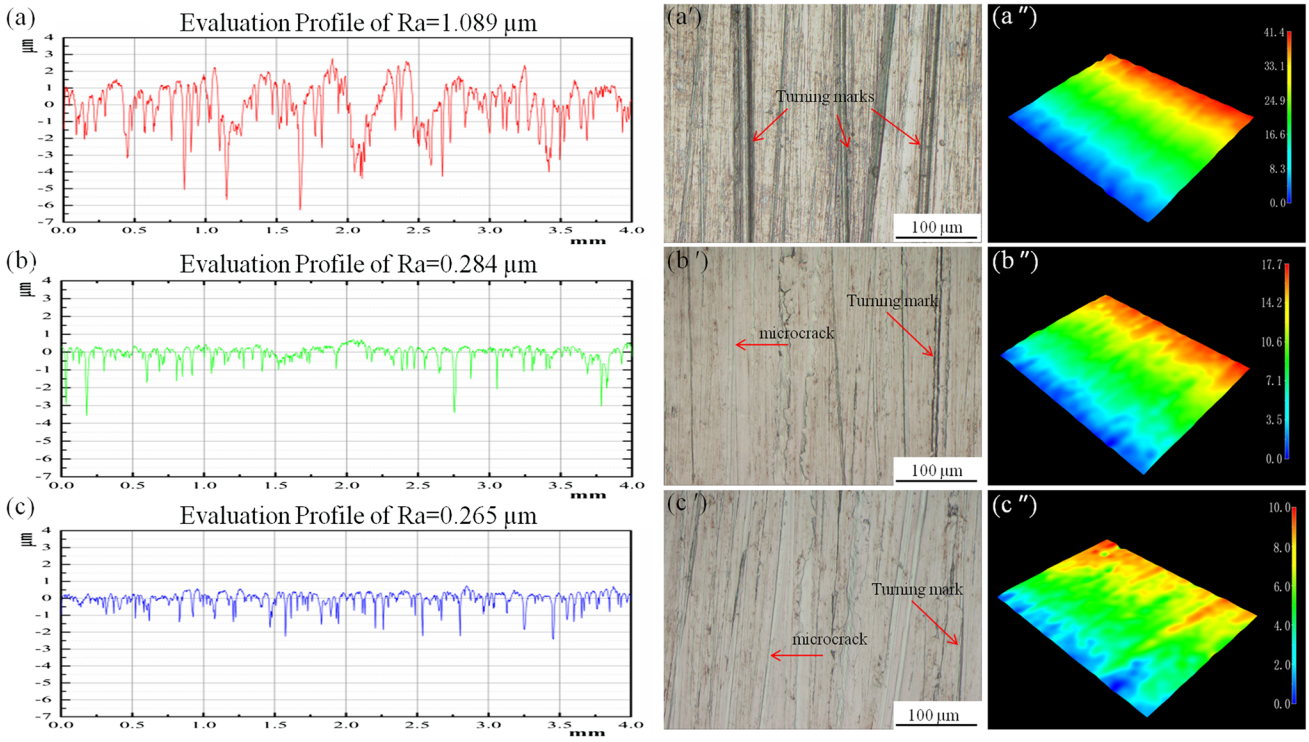

Fig. 2 The axial surface roughness and morphology of turning, USRP and UDCT samples (a, a′, a″) turning; (b, b′, b″) USRP; (c, c′, c″) UDCT

affecting the fatigue life of the steel (Ref 31). When USRP is applied, the depth and number of the turning marks are significantly reduced. Some shallow turning marks became microcracks after USRP, as shown in Fig. 2(b′). The existing studies indicate that USRP can reduce surface roughness (Ref 7, 32, 33). When DCT is applied, the distribution and morphology of carbides is more uniform throughout the matrix (Fig. 5d). The uniformity and homogeneity in carbide distribution and morphology lead to lower values of surface roughness (Ref 34). Thus, it can be found that the depth of the turning marks and the quantity of the microcracks can be further reduced when UDCT is introduced (Fig. 2c′). After UDCT, the surface is smoother with fewer cracks and defects. The 3D micromorphologies of the three samples also confirm this process. The evolution of the micromorphologies of machined surface shows that UDCT can facilitate cracks healing and reduce defects to further improve the surface quality.

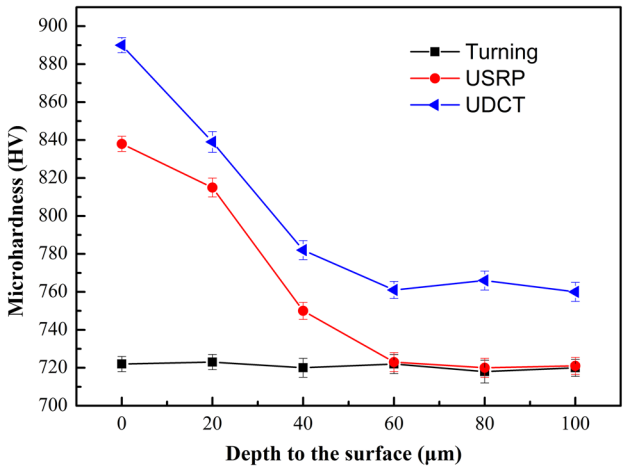

Fig. 3 Cross-sectional hardness gradient distribution within the surface-strengthened layer of turning, USRP and UDCT samples

3.2 Microindentation Hardness

The cross-sectional microindentation hardness distribution within the strengthened layer induced by USRP and UDCT was carefully measured. The variations of cross-sectional hardness gradient are presented in Fig. 3. It can be seen from Fig. 3 that the original microindentation hardness of the quenched and tempered Cr12MoV is about 720 HV, which is expressed as a black line in Fig. 3. After USRP and UDCT, the surface microindentation hardness receives a significant improvement. For USRP samples, the surface microindentation hardness

increases from the initial state ~ 720 to ~ 838 HV. This indicates an increase in rate of 16.4%, which can be attributed to grain refinement and work hardening during the rolling process. The surface hardness of USRP samples decreases rapidly as the depth increase and is eventually stabilized to ~ 720 HV. For UDCT samples, the surface microindentation hardness increases from the USRP state ~ 838 to ~ 890 HV, which indicates an increase in rate of 6.2%, compared with USRP samples. The microindentation hardness of the UDCT samples is also decreased rapidly, but its stable hardness increases to 760 HV. In other words, compared with USRP samples, the microindentation hardness of UDCT samples shows an overall improvement with an average value of 40 HV. It can be seen that performing DCT after USRP can increase the sample hardness significantly, which may be attributed to the microstructure evolution during UDCT.

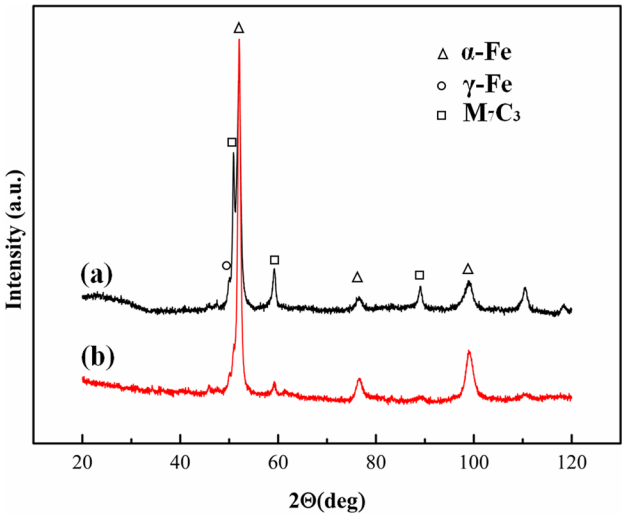

Fig. 4 X-ray diffraction patterns of (a) turning and (b) UDCT samples

3.3 XRD

The x-ray diffraction patterns of the turning and UDCT samples are illustrated in Fig. 4. The XRD patterns of the two samples reveal peaks of M_7C_3 carbide, martensite (α-Fe), as well as small peaks of RA (γ-Fe). It can be seen that the diffraction maximums of RA are decreased extremely with the increase in the diffraction maximums of martensite after DCT. The volume fractions of the RA in the turning and UDCT samples are 13 and 7%, respectively. The decrease in RA and the increase in martensite indicate the martensitic transformation of RA, promoting an increase in wear resistance and hardness.

3.4 Microstructure

The microstructure evolution induced by USRP and UDCT is demonstrated in Fig. 5. Figure 5(a) presents the quenched and tempered microstructure of Cr12MoV. It shows an irregular distribution of grains with random orientation. After USRP, a

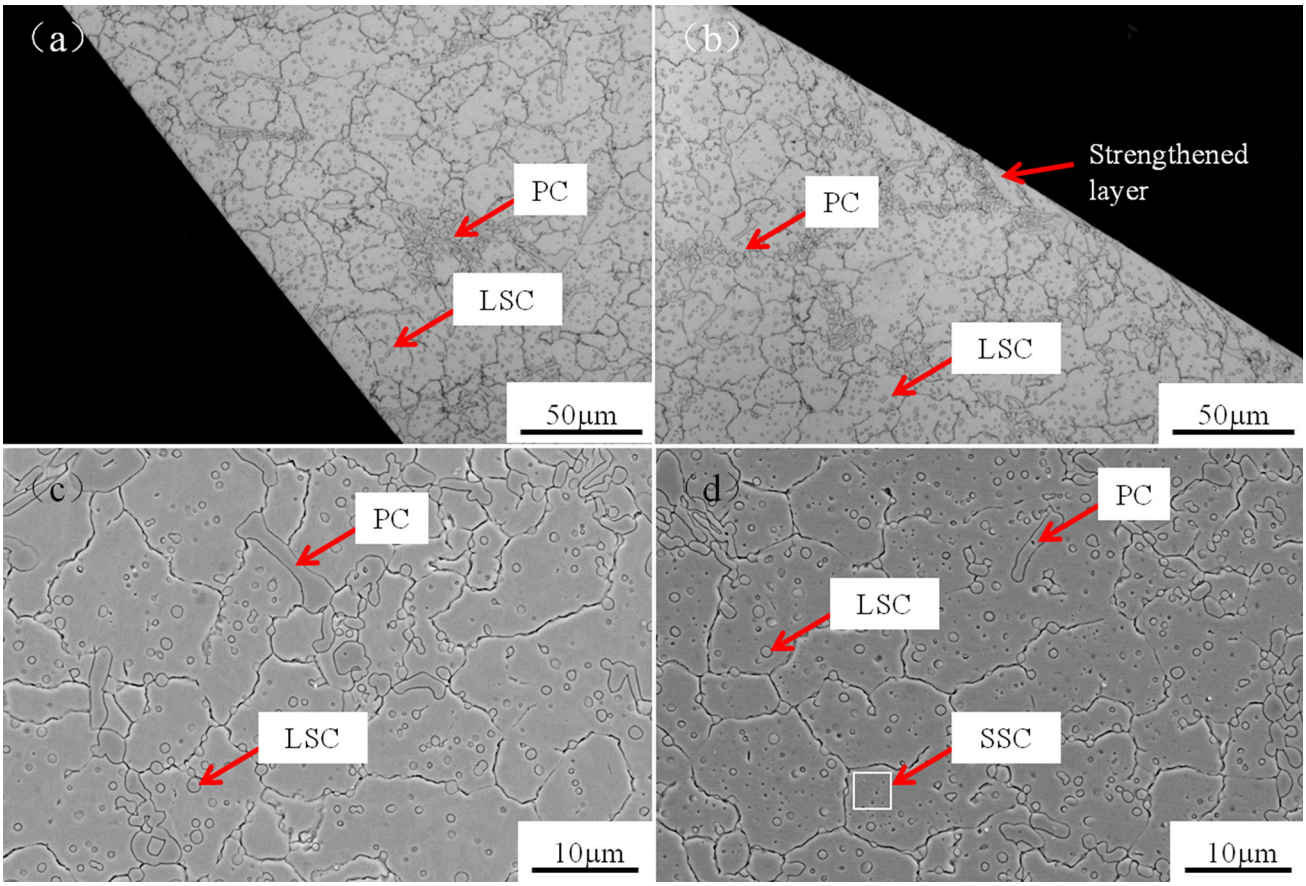

Fig. 5 Cross section metallographs of turning (a) and USRP (b) samples and SEM micrographs of USRP (c) and UDCT (d) samples

strengthened layer with a depth of about 20 μm appears on the top surface of Cr12MoV (Fig. 5b). Meanwhile, there are a large number of nonstandard carbides in the matrix of the quenched and tempered Cr12MoV, just as depicted in Fig. 5(c). Carbide particles are classified as primary carbides (PC) and secondary carbides (SC). SCs are further classified as large secondary carbides (LSC) and small secondary carbides (SSC), which are considered in the nanoscale. The size of the LSC is between 1 and 5 μm, while the size of the PC is greater than 5 μm. Justification for the classification of carbides and selection of the size limits have been reported by Torkamani (Ref 35) and Das et al. (Ref 18). It can be seen that the carbides in the matrix are mainly PCs and LSCs before DCT (Fig. 5c). After DCT is applied, a large number of SSCs are precipitated from the matrix (Fig. 5d). Furthermore, the precipitation positions of SSCs are mainly concentrated in the gap of LSCs, which leads to a more uniform distribution of carbides in the matrix. Thus, UDCT could produce a strengthened layer with more SSCs and a more homogenous distribution of carbides than USRP, which is conducive to excellent surface properties.

3.5 Friction and Wear

The weight loss of the turning, USRP and UDCT samples after friction was measured and is listed in Table 3. It is observed that USRP and UDCT samples have higher wear resistance. The weight loss of USRP and UDCT samples is only about 1/5 and 1/8 of that of the turning samples, respectively. Figure 6 indicates the curves of friction coefficient μ of the turning, USRP and UDCT samples. It can be observed that, during the whole friction process, the friction coefficient μ of USRP and UDCT samples is overall lower than that of the turning samples. The friction coefficient μ of the three samples is relatively high at the beginning of the friction. This may be due to the fact that the oil protective films between the friction pairs have not yet been formed, and dry friction plays a leading role. With the friction time increase, the oil protective films gradually form and the friction coefficient gradually decreases to a stable level with the turning sample of 0.211, USRP sample of 0.203 and UDCT sample of 0.201. Obviously, the UDCT sample has the lowest value. The friction coefficient of the three samples becomes higher after long time friction, which may be attributed to the abrasion of the samples. Consequently, UDCT and USRP can obviously improve the wear resistance, probably because of the high hardness and low surface roughness.

Table 3 Weight comparison of turning, USRP and UDCT samples

Sample	Before test, g	After test, g	Weight loss, g
Truning	198.2466	198.2301	0.0165
USRP	199.3785	199.3749	0.0036
UDCT	200.8231	200.8202	0.0023

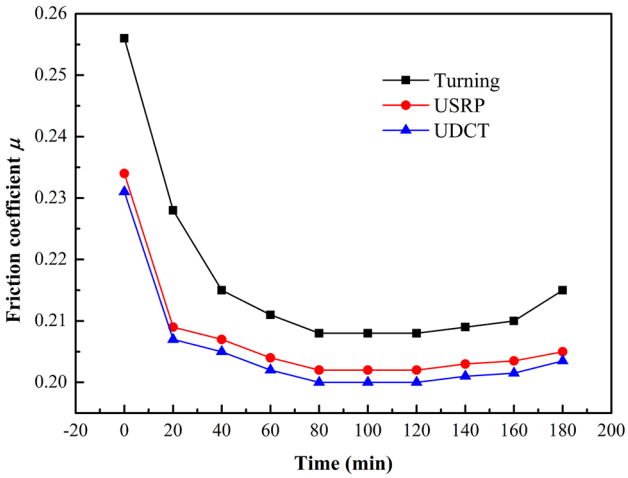

Fig. 6 Comparison of friction coefficient variation

4. Discussion

It is well known that the enhanced mechanical properties are closely related to microstructure refinement. In the present study, the refinement is mainly induced by deformation. During USRP, serve plastic deformation is brought into the surface layer due to serious extrusion caused by high-frequency collision of rolling tip. During the rolling process, the time interval between two ball-to-sample collisions, 30 kHz here, is short enough to be insufficient for elastic recovery. Therefore, the overlap of multiple elastic deformations would result in plastic compression deformation, even if the stress value of the rolling equipment is less than the yield strength. The metallographic structure of the turning samples is martensite matrix, a small amount of RA and carbides, as shown in Fig. 5(a). The martensite is body-centered tetragonal structure which has 48 slip systems. In addition, the stacking faults energy of Cr12MoV is very high. Hence, plastic deformation takes place primarily by multi-slip and inter-slip, that is, dislocation movements. As the number of rolling cycles increases, the dislocations in grains are increased. Then the high-density dislocation walls and dislocation entanglements are formed through dislocation propagation, slip, annihilation and recombination, which would gradually turn into small-angle subgrain boundaries. With the further increase in the strain, the angle of subgrain boundaries is increased; then the grain size is reduced and misorienation is increased. When the generating and annihilating rates of dislocations become equilibrium, equiaxed and stable nano-grains possessing random orientations are eventually formed (Ref 36, 37). At this time, hardness and grain refining are extremely enhanced during the repeat striking. However, the significant hardening in surface-strengthened layer induced by severe plastic deformation becomes an obstruct for the further plastic deformation, during the severe striking process (Ref 32). The severe deformation limitation would cause the introduction of large amounts of immobile dislocations and boundaries, which would restrict the further grain refinement (Ref 38). It is necessary to apply great stress on the sample to make these immobile dislocations or boundaries turn into subgrains. During USRP, deformation takes place both inside the grain and on the boundary. Deformation first occurs mainly inside the grain as the interior deforms more easily than the boundary at low temperatures. With the further increase in the strain, the grain boundaries begin to rotate or slide (Ref 39). As for grains with different orientations, the slip systems that can be activated to vary from

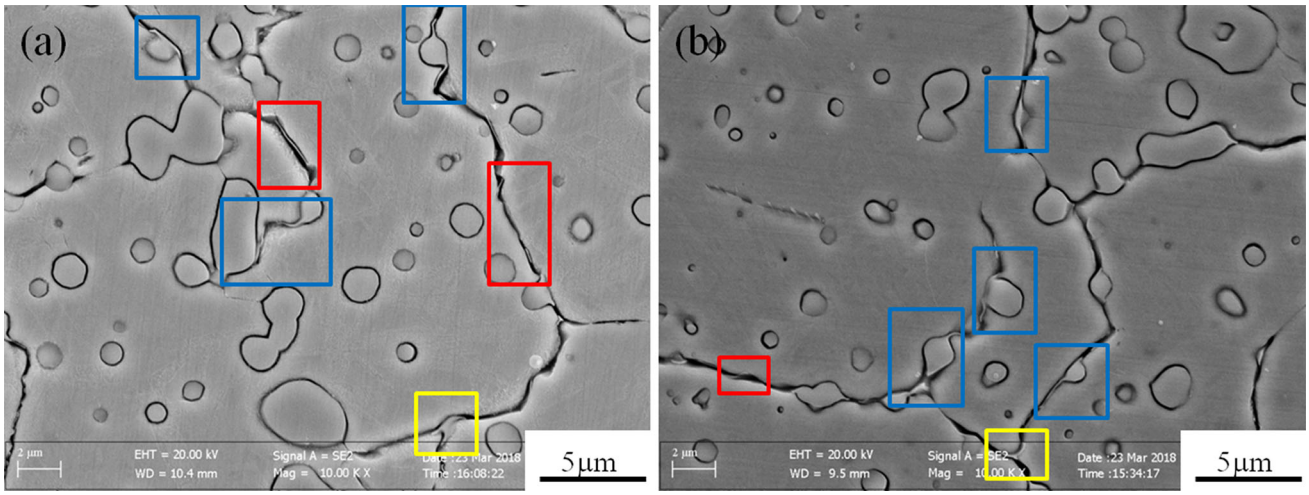

Fig. 7 SEM maps of the distribution of retained austenite of (a) USRP; (b) UDCT samples. The boxes are colored as follows: red box = ORA; yellow box = TRA; blue box = CRA (Color figure online)

each other, so the dislocation density and orientations are quite different. Therefore, the morphology of the grain boundary changes with the depth to the surface. In the present study, as the hardness of the quenched and tempered Cr12MoV is about 720 HV and the static force that applied on the sample surface is 1246 N, the work hardening of the surface has a greater impact on the further hardening. The force exerted on the surface of the turning samples is not sufficient to form cellular structures. Thus, no subgrain boundary is formed in this study, but the grain boundary deforms along the rolling direction (Fig. 5b). Although the rolling force is insufficient to form subgrains, high-density dislocations are formed on the surface of the grains, which also enhance the surface strength. The depth of the strengthened layer is only about 20 μm (Fig. 5b), which is more shallow than that in Ref 7 and 33.

As stated earlier, a large number of carbides are distributed in the quenched and tempered Cr12MoV. USRP not only increases the dislocation density, changes the morphology of the grain boundary, but also changes the distribution of carbides. Due to the good cooling conditions during USRP, the rise of temperature is low. During the whole process, the sample temperature remains below 200 °C which is not enough to cause dissolution or precipitation of carbides. Therefore, USRP only changes the distribution of carbides mechanically. During USRP, serve plastic deformation leads to the decrease in the grain size on the surface of the sample (from about 30 μm to less than 10 μm). In most cases, the relation between strength/hardness and grain size can be described by the Hall–Petch relation:

$$\sigma = \sigma_0 + k_d d^{-1/2} \quad \text{(Eq 1)}$$

where σ_0 is the lattice friction stress required to move individual dislocations, k_d is a material-dependent constant known as the Hall–Petch slope and d is the average grain size (Ref 40). It is obvious that the reduction in the grain size on the surface can increase the surface hardness of the sample. In addition, the reduction in the grain size on the surface results in an increase in carbides per unit grain on the surface of the sample, thus increasing the surface hardness of the sample to some extent (Ref 41). At the same time, the carbides (mainly SCs) inside the grains are linearly distributed along the surface of the sample, as the grains of surface layer are rod-shaped. In addition, the block and inhomogeneously distributed PCs in the grains are broken by the high-frequency collision. The fine and uniform distribution of PCs facilitate the enhancement of hardness and wear resistance (Ref 42). In summary, the increase in the surface hardness and wear resistance can be attributed to the high-density dislocations, carbides and the fragmentation of partial PCs.

The hardness and wear resistance were further improved by UDCT. DCT can increase the hardness of the samples mainly for two reasons. On the one hand, DCT leads to transformation of RA to martensite, which increases the content of martensite, thus improving the hardness. In the present study, the contents of RA that transformed by DCT is 6%, and there is still 7% of RA remains untransformed. This is in agreement with the report that only a fraction of RA can be transformed into martensite during DCT (Ref 43, 44). The martensite transformation increases the stability of the surface of the sample, leading to a smaller change in the size of the sample during the long-time service life. The distribution of RA before and after DCT is shown in Fig. 7. RA is sorted as ordinary retained austenite (ORA), triple retained austenite (TRA) and carbides retained austenite (CRA), according to the location of RA. The ORA is located on ordinary grain boundary, as shown in the red box in Fig. 7. The TRA is located on the intersection of three grain boundaries, as shown in the yellow box in Fig. 7. The CRA is located on the intersection of carbides and grain boundaries, as shown in the blue box in Fig. 7. It can be seen from Fig. 7 that the decrease in RA is mainly due to the reduction in ORA, and there is no obvious change in the content of TRA and CRA. The fracture of the steel during service life is mainly caused by stress concentration near PCs and the triple grain boundaries (Ref 17, 45). The representative SEM fractographs of turning and UDCT samples are shown in Fig. 8. Figure 8(a) shows that a crack in the quenched and tempered Cr12MoV is initiated by PC and extended to the matrix, which indicates the stress concentration on/near PCs. Figure 8(b) presents that cracks are located in the intersection of three grain boundaries, which indicates the stress concentration in the triple grain boundaries. The remaining small amount of RA, mainly TRA and CRA, can reduce the stress concentration and thus improve wear resistance.

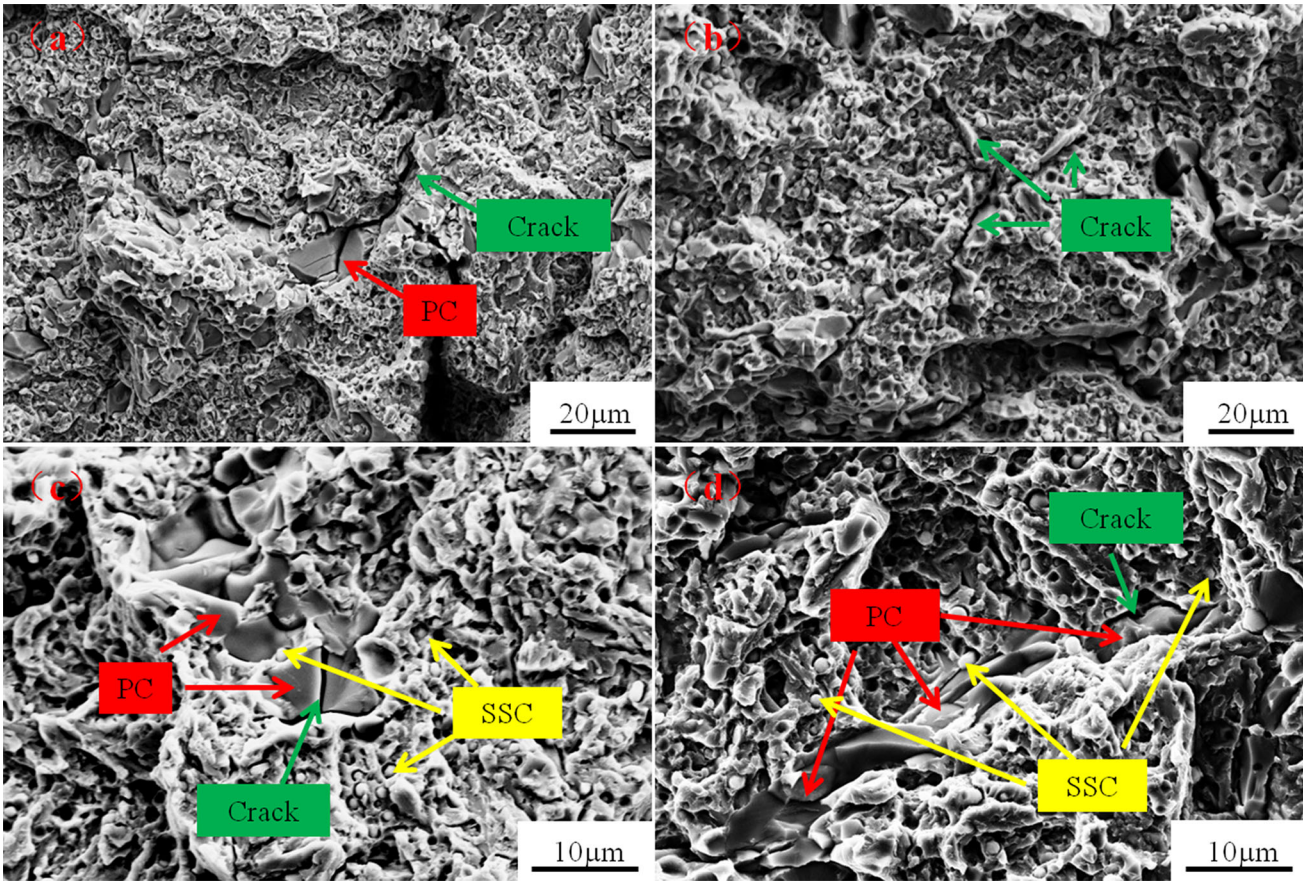

Fig. 8 SEM fractographs of (a, b) turning and (c, d) UDCT samples

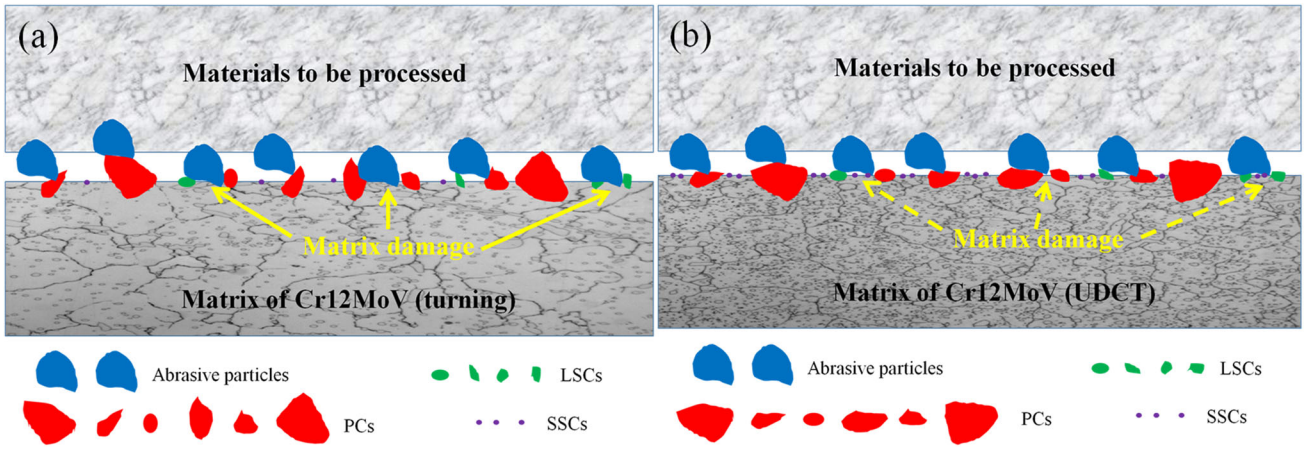

Fig. 9 Scheme of particle attrition in (a) turning and (b) UDCT samples

On the other hand, the lattice shrinkage of the martensite and austenite at low temperatures during DCT reduces the carbon content in martensite. A high internal stress state is generated during the quenching and cryogenic stages due to thermal stresses and the transformation of austenite into martensite (Ref 46, 47). In addition, the internal stress of the sample surface was further enhanced during USRP. Therefore, the enhanced internal stresses give rise to a large number of structural defects during DCT and the carbon-supersaturated martensite becomes unstable (Ref 44). Then the carbon atoms are forced to diffuse toward the recently created defects and make new carbide nucleus. This process is in virtue of two different mechanisms: a short-range diffusion mechanism (Ref 46) and a consequence of the capture and transport of carbon atoms by moving dislocations (Ref 48). As a result, the martensite is decomposed and carbide precipitation initiates which increases the carbide percentages and the homogenous distribution (Ref 22). Due to the numerous defects that are induced by USRP and thermal stresses and the slow diffusion of carbon atoms at low temperatures, the carbides of this new nucleation are in

nanoscale. These nano-sized carbides can play a dispersion strengthening role in the martensite matrix, thus improving the hardness (Ref 49). In addition, the precipitation position of SSCs is mainly concentrated in the gap of PCs and SCs, namely a more homogenous distribution of carbides is obtained during DCT. There is no doubt that the homogenous distribution can promote the hardness and wear resistance (Ref 50). Figure 8(c) and d shows the fractographs of UDCT samples. It can be seen from Fig. 8(c) and (d) that there is a lot of SSCs near PC. The presence of these SSCs can alleviate the stress concentration around the PC. That is why there is a crack on the PC (Fig. 8c), but it does not extend to the matrix. There are even no cracks near the chain PCs (Fig. 8d). The scheme of particle attrition in turning and UDCT samples is shown in Fig. 9. As can be seen, there are some matrix damages on the surface of the turning sample, due to the inhomogenous distribution of PCs and SCs. The matrix damage is mainly located in the gap between PC and SCs (Fig. 9a). During UDCT, the PCs and SCs were linearly distributed along the surface of the sample under the action of USRP and lots of SSCs precipitated in the gap between PC and SCs under the action of DCT. Thus, the abrasive particles are hard to wear the matrix. The matrix damage is greatly reduced (Fig. 9b). Therefore, the further increase in the hardness and wear resistance are mainly attributed to the martensite transformation, the dispersion strengthening of SSCs and the homogenized carbides distribution during UDCT.

5. Conclusions

The surface mechanical properties and microstructure evolution of quenched and tempered cold work die steel Cr12MoV during USRP and UDCT were carefully studied in the present work. The results indicated that UDCT had more advantages over USRP in achieving excellent machined surface quality with the surface roughness decreased from ~ Ra 0.284 to ~ Ra 0.265, improving surface Vickers microindentation hardness from ~ 838 to ~ 890 HV with an increase of 6.2% and enhancing surface wear resistance with a lower coefficient and less weight loss. These enhancements in mechanical behaviors are closely related to the microstructure evolution induced by UDCT. That is, under the coupling effects of USRP and DCT, martensitic transformation of RA, the dispersion strengthening of SSCs and the homogenized carbides distribution are the main reasons for the observed phenomena. Therefore, UDCT provides a highly efficient approach to prepare excellent surface mechanical properties of Cr12MoV.

References

1. Z.B. Wang, N.R. Tao, S. Li, W. Wang, G. Liu, J. Lu, and K. Lu, Effect of Surface Nanocrystallization on Friction and Wear Properties in Low Carbon Steel, *Mater. Sci. Eng., A*, 2003, **352**(1–2), p 144–149
2. L.L. Shaw, Enhanced Fatigue Resistance of a Nickel-Based Hastelloy Induced by a Surface Nanocrystallization and Hardening Process, *Philos. Mag. Lett.*, 2005, **85**(8), p 427–438
3. G. Li, S.G. Qu, Y.X. Pan, and X.Q. Li, Effects of the Different Frequencies and Loads of Ultrasonic Surface Rolling on Surface Mechanical Properties and Fretting Wear Resistance of HIP Ti-6Al-4V alloy, *Appl. Surf. Sci.*, 2016, **389**, p 324–334
4. X.J. Cao, Y.S. Pyoun, and R. Murakami, Fatigue Properties of a S45C Steel Subjected to Ultrasonic Nanocrystal Surface Modification, *Appl. Surf. Sci.*, 2010, **256**(21), p 6297–6303
5. A. Amanov, I.S. Cho, and Y.S. Pyun, Microstructural Evolution and Surface Properties of Nanostructured Cu-Based Alloy by Ultrasonic Nanocrystalline Surface Modification Technique, *Appl. Surf. Sci.*, 2016, **388**, p 185–195
6. A. Amanov, J.H. Kim, Y.S. Pyun, T. Hirayama, and M. Hino, Wear Mechanisms of Silicon Carbide Subjected to Ultrasonic Nanocrystalline Surface Modification Technique, *Wear*, 2014, **332–333**, p 891–899
7. T. Wang, D. Wang, G. Liu, B. Gong, and N. Song, Investigations on the Nanocrystallization of 40Cr Using Ultrasonic Surface Rolling Processing, *Appl. Surf. Sci.*, 2008, **255**(5), p 1824–1829
8. H.W. Huang, Z.B. Wang, J. Lu, and K. Lu, Fatigue Behaviors of AISI, 316L Stainless Steel with a Gradient Nanostructured Surface Layer, *Acta Mater.*, 2015, **87**, p 150–160
9. A.V. Panin, M.S. Kazachenok, A.I. Kozelskaya, R.R. Hairullin, and E.A. Sinyakova, Mechanisms of Surface Roughening of Commercial Purity Titanium During Ultrasonic Impact Treatment, *Mater. Sci. Eng., A*, 2015, **647**, p 43–50
10. H. Wang, G. Song, and G. Tang, Effect of Electropulsing on Surface Mechanical Properties and Microstructure of AISI, 304 Stainless Steel During Ultrasonic Surface Rolling Process, *Mater. Sci. Eng., A*, 2016, **662**, p 456–467
11. Z. Sun, H. Wang, Y. Ye, Z. Xu, and G. Tang, Effects of Electropulsing on the Machinability and Microstructure of GH4169 Superalloy During Turning Process, *Int. J. Adv. Manuf. Technol.*, 2018, **95**(5–8), p 2835–2842
12. X. Li, F. Wang, X. Li, G. Tang, and J. Zhu, Improvement of Formability of Mg-3Al-1Zn Alloy Strip by Electroplastic-Differential Speed Rolling, *Mater. Sci. Eng., A*, 2014, **618**, p 500–504
13. J. Kuang, X. Du, X. Li, Y. Yang, A.A. Luo, and G. Tang, Athermal Influence of Pulsed Electric Current on the Twinning Behavior of Mg-3Al-1Zn Alloy During Rolling, *Scripta Mater.*, 2016, **114**, p 151–155
14. R. Zhu, G. Tang, S. Shi, and M. Fu, Effect of Electroplastic Rolling on Deformability and Oxidation of NiTiNb Shape Memory Alloy, *J. Mater. Process. Technol.*, 2013, **213**(1), p 30–35
15. Q. Xu, L. Guan, Y. Jiang, G. Tang, and S. Wang, Improved Plasticity of Mg-Al-Zn Alloy by Electropulsing Tension, *Mater. Lett.*, 2010, **64**(9), p 1085–1087
16. R.S. Qin, A. Rahnama, W.J. Lu, X.F. Zhang, and B. Elliottbowman, Electropulsed Steels, *Mater. Sci. Technol.*, 2014, **30**(9), p 1040
17. H. Li, W. Tong, J. Cui, H. Zhang, L. Chen, and L. Zuo, The Influence of Deep Cryogenic Treatment on the Properties of High-Vanadium Alloy Steel, *Mater. Sci. Eng., A*, 2016, **662**, p 356–362
18. D. Das, A.K. Dutta, and K.K. Ray, Sub-Zero Treatments of AISI, D2 Steel: Part I. Microstructure and Hardness, *Mater. Sci. Eng., A*, 2010, **527**(9), p 2182–2193
19. D. Das, A. Dutta, and K. Ray, On the Refinement of Carbide Precipitates by Cryotreatment in AISI, D2 Steel, *Phil. Mag.*, 2009, **89**(1), p 55–76
20. Y. He, K. Yang, W. Qu, F. Kong, and G. Su, Strengthening and Toughening of a 2800-MPa Grade Maraging Steel, *Mater. Lett.*, 2002, **56**(5), p 763–769
21. F.J.D. Silva, S.D. Franco, Á.R. Machado, E.O. Ezugwu, and A.M.S. Jr., Performance of Cryogenically Treated HSS Tools, *Wear*, 2006, **261**(5), p 674–685
22. S. Zhirafar, A. Rezaeian, and M. Pugh, Effect of Cryogenic Treatment on the Mechanical Properties of 4340 Steel, *J. Mater. Process. Technol.*, 2007, **186**(1–3), p 298–303
23. V. Leskovšek, M. Kalin, and J. Vižintin, Influence of Deep-Cryogenic Treatment on Wear Resistance of Vacuum Heat-Treated HSS, *Vacuum*, 2006, **80**(6), p 507–518
24. H. Liu, J. Wang, H. Yang, and B. Shen, Effects of Cryogenic Treatment on Microstructure and Abrasion Resistance of CrMnB High-Chromium Cast Iron Subjected to Sub-critical Treatment, *Mater. Sci. Eng., A*, 2008, **478**(1–2), p 324–328
25. K.S. Ayl Yong and M. Rahman, Performance Evaluation of Cryogenically Treated Tungsten Carbide Tools in Turning, *Int. J. Mach. Tools Manuf*, 2006, **46**(15), p 2051–2056
26. M. Preciado, P.M. Bravo, and J.M. Alegre, Effect of Low Temperature Tempering Prior Cryogenic Treatment on Carburized Steels, *J. Mater. Process. Technol.*, 2006, **176**(1), p 41–44

27. K. Amini, S. Nategh, and A. Shafyei, Influence of Different Cryotreatments on Tribological Behavior of 80CrMo12 5 Cold Work Tool Steel, *Mater. Des.*, 2010, **31**(10), p 4666–4675
28. R. Thornton, T. Slatter, A.H. Jones, and R. Lewis, The Effects of Cryogenic Processing on the Wear Resistance of Grey Cast Iron Brake Discs, *Wear*, 2011, **271**(9–10), p 2386–2395
29. A. Molinari, M. Pellizzari, S. Gialanella, G. Straffelini, and K.H. Stiasny, Effect of Deep Cryogenic Treatment on the Mechanical Properties of Tool Steels, *J. Mater. Process. Technol.*, 2001, **118**(1–3), p 350–355
30. Y. Dong, X.P. Lin, and H.S. Xiao, Deep Cryogenic Treatment of High-Speed Steel and Its Mechanism, *Heat Treat. Met.*, 1998, **25**(3), p 55–59
31. W. Zhuang, Q. Liu, R. Djugum, P.K. Sharp, and A. Paradowska, Deep Surface Rolling for Fatigue Life Enhancement of Laser Clad Aircraft Aluminium Alloy, *Appl. Surf. Sci.*, 2014, **320**(320), p 558–562
32. H. Wang, G. Song, and G. Tang, Evolution of Surface Mechanical Properties and Microstructure of Ti 6Al 4 V Alloy Induced by Electropulsing-Assisted Ultrasonic Surface Rolling Process, *J. Alloy. Compd.*, 2016, **681**, p 146–156
33. H. Wang, G. Song, and G. Tang, Enhanced Surface Properties of Austenitic Stainless Steel by Electropulsing-Assisted Ultrasonic Surface Rolling Process, *Surf. Coat. Technol.*, 2015, **282**, p 149–154
34. N.B. Dhokey and P.K. Lalge, Influence of Cryosoaking Period on Wear Characteristics and Surface Topography of M35 Tool Steel, *Tribol. Mater. Surf. Interfaces*, 2018, **12**, p 170–175
35. H. Torkamani, S. Raygan, and J. Rassizadehghani, Comparing Microstructure and Mechanical Properties of AISI, D2 Steel After Bright Hardening and Oil Quenching, *Mater. Des.*, 2014, **54**, p 1049–1055
36. J.Y. Huang, Y.T. Zhu, H. Jiang, and T.C. Lowe, Microstructures and Dislocation Configurations in Nanostructured Cu Processed by Repetitive Corrugation and Straightening, *Acta Mater.*, 2001, **49**(9), p 1497–1505
37. K. Lu and J. Lu, Nanostructured Surface Layer on Metallic Materials Induced by Surface Mechanical Attrition Treatment, *Mater. Sci. Eng., A*, 2004, **375–377**(1), p 38–45
38. X.C. Liu, H.W. Zhang, and K. Lu, Strain-Induced Ultrahard and Ultrastable Nanolaminated Structure in Nickel, *Science*, 2013, **342**(6156), p 337–340
39. N.A. Mara, A.V. Sergueeva, T.D. Mara, S.X. Mcfadden, and A.K. Mukherjee, Superplasticity and Cooperative Grain Boundary Sliding in Nanocrystalline Ni3Al, *Mater. Sci. Eng., A*, 2007, **463**(1), p 238–244
40. S. Ren, Z. Sun, Z. Xu, R. Xin, J. Yao, D. Lv, and J. Chang, Effects of Twins and Precipitates at Twin Boundaries on Hall-Petch Relation in High Nitrogen Stainless Steel, *J. Mater. Res.*, 2018, **33**(12), p 1764–1772
41. H.G. Nanesa, J. Boulgakoff, and M. Jahazi, Influence of Prior Cold Deformation on Microstructure Evolution of AISI, D2 Tool Steel After Hardening Heat Treatment, *J. Manuf. Process*, 2016, **22**, p 115–119
42. M.A. Hamidzadeh, M. Meratian, and M.M. Zahrani, A Study on the Microstructure and Mechanical Properties of AISI, D2 Tool Steel Modified by Niobium, *Mater. Sci. Eng., A*, 2010, **556**(12), p 758–766
43. S. Li, Y. Xie, and X. Wu, Hardness and Toughness Investigations of Deep Cryogenic Treated Cold Work Die Steel, *Cryogenics*, 2010, **50**(2), p 89–92
44. M. Pérez and F.J. Belzunce, The Effect of Deep Cryogenic Treatments on the Mechanical Properties of an AISI, H13 Steel, *Mater. Sci. Eng., A*, 2015, **624**, p 32–40
45. T.V. Pirtovšek, G. Kugler, and M. Terčelj, The Behaviour of the Carbides of Ledeburitic AISI, D2 Tool Steel During Multiple Hot Deformation Cycles, *Mater. Charact.*, 2013, **83**(3), p 97–108
46. D. Senthilkumar, I. Rajendran, M. Pellizzari, and J. Siiriainen, Influence of Shallow and Deep Cryogenic Treatment on the Residual State of Stress of 4140 Steel, *J. Mater. Process. Technol.*, 2011, **211**(3), p 396–401
47. K. Amini, A. Akhbarizadeh, and S. Javadpour, Investigating the Effect of Holding Duration on the Microstructure of 1.2080 Tool Steel During the Deep Cryogenic Heat Treatment, *Vacuum*, 2012, **86**(10), p 1534–1540
48. A.I. Tyshchenko, W. Theisen, A. Oppenkowski, S. Siebert, O.N. Razumov, A.P. Skoblik, V.A. Sirosh, Y.N. Petrov, and V.G. Gavriljuk, Low-Temperature Martensitic Transformation and Deep Cryogenic Treatment of a Tool Steel, *Mater. Sci. Eng., A*, 2010, **527**(26), p 7027–7039
49. P. Jurči, M. Dománková, Ľ. Čaplovič, J. Ptačinová, J. Sobotová, P. Salabová, O. Prikner, B. Šuštaršič, and D. Jenko, Microstructure and Hardness of Sub-Zero Treated and No Tempered P/M Vanadis 6 Ledeburitic Tool Steel, *Vacuum*, 2015, **111**, p 92–101
50. G.A. Fontalvo, R. Humer, C. Mitterer, K. Sammt, and I. Schemmel, Microstructural Aspects Determining the Adhesive Wear of Tool Steels, *Wear*, 2006, **260**(9–10), p 1028–1034